Modeling of space-time focusing of localized nondiffracting pulses

Michel Zamboni-Rached[1,2] and Ioannis M. Besieris[3]
[1]*School of Electrical and Computer Engineering, University of Campinas, Campinas, SP, Brazil*
[2]*Department of Electrical and Computer Engineering, University of Toronto, Toronto, ON, Canada*
[3]*The Bradley Department of Electrical and Computer Engineering, Virginia Polytechnic Institute and State University, Blacksburg, Virginia 24060, USA*
(Received 30 September 2015; published 12 October 2016)

In this paper we develop a method capable of modeling the space-time focusing of nondiffracting pulses. These pulses can possess arbitrary peak velocities and, in addition to being resistant to diffraction, can have their peak intensities and focusing positions chosen *a priori*. More specifically, we can choose multiple locations (spatial ranges) of space and time focalization; also, the pulse intensities can be chosen in advance. The pulsed wave solutions presented here can have very interesting applications in many different fields, such as free-space optical communications, remote sensing, medical apparatus, etc.

DOI: 10.1103/PhysRevA.94.043811

I. INTRODUCTION

It is well known that the scalar wave equation, in particular, and more generally Maxwell's equations have very interesting classes of solutions named nondiffracting waves [1–10], also called localized waves. These beams and pulses are immune to diffraction effects but have the drawback of containing infinite energy. This problem, however, can be solved [4,6,11–13] and the finite-energy versions of the ideal nondiffracting waves can resist the diffraction effects for long (finite) distances when compared to the ordinary waves.

In this paper, we take a step forward in the theory of the nondiffracting pulses by introducing a method that enables us to perform a space and time modeling on them. In other words, we can construct nondiffracting localized pulse solutions in such a way that we can choose where and how intense their peaks will be within a longitudinal spatial range $0 \leqslant z \leqslant L$. This is not just an ordinary focusing method [14–16], where there is just one point of focalization; actually, it is a much more powerful method because it allows the choice of multiple locations (spatial ranges) of space and time focalization where the pulse intensities also can be chosen *a priori*.

Such modeling of the space and time evolution of ideal localized nondiffracting pulses with subluminal, luminal, or superluminal peak velocities is made through a suitable and discrete superposition of ideal standard nondiffracting pulses. As a consequence, the resulting solutions also present infinite energy content. Finite-energy space-time focused solutions can be achieved by replacing the ideal nondiffracting pulses with their finite-energy versions in the fundamental superposition followed by specific changes in the respective series coefficients.

The resulting waves can possess potential applications in many different fields, such as free-space optical communications, remote sensing, medical apparatus, etc.

In Sec. II we present important results related to ideal nondiffracting pulses characterized by azimuthal symmetry, with the bidirectional and unidirectional decomposition approaches playing important roles. Section III is devoted to the modeling of the space-time focusing of localized nondiffracting pulses and examples are presented to confirm the efficiency of the method. The finite-energy version of the space-time focusing theory is discussed in Sec. IV. Section V is devoted to the conclusions.

II. IMPORTANT POINTS RELATED TO THE IDEAL (STANDARD) NONDIFFRACTING PULSES

In this section we present several important points regarding the ideal nondiffracting pulses, stressing the importance of the bidirectional and unidirectional decomposition methods used to derive closed analytical solutions describing such waves. Here, we do not enter into mathematical details and demonstrations, as this subject has already been very well developed in a series of papers [6,11–13].

Considering only propagating waves and azimuthal symmetry, the general solution to the homogeneous scalar wave equation, $\Box\psi = 0$ (with $\Box$ being the d'Alembertian), can be written in cylindrical coordinates as

$$\psi(\rho,z,t) = \int_{-\infty}^{\infty} d\omega \int_{-\infty}^{\infty} dk_z \int_0^{\infty} k_\rho \, dk_\rho \, A'(k_\rho,k_z,\omega) \times \delta\left(k_\rho^2 - \left(\frac{\omega^2}{c^2} - k_z^2\right)\right) J_0(k_\rho\rho) e^{ik_z z} e^{-i\omega t} \quad (1)$$

with $A'(k_\rho,k_z,\omega)$ being an arbitrary function and $\delta(\cdot)$ the Dirac delta function. The integral solution (1) is nothing but a superposition of zero-order Bessel beams involving the angular frequency (ω) and the transverse (k_ρ) and longitudinal (k_z) wave numbers.

It is well known [6,11–13] that an ideal nondiffracting pulse with peak velocity $0 \leqslant V \leqslant \infty$ can be obtained when the spectrum $A'(k_\rho,k_z,\omega)$ forces a coupling of the type $\omega = Vk_z + b$, with b a constant, between the angular frequency and the longitudinal wave number. Such a coupling, and the solutions resulting from it, can be much more easily obtained when the bidirectional or unidirectional decompositions [6,11–13] are adopted. These are characterized by changes from the spatial (z) and time (t) coordinates to the new ones, ζ and η, given by

$$\zeta = z - Vt, \quad \eta = z + ut \quad (2)$$

with $V > 0$ and $\forall u \neq -V$. The transformation (2) is called bidirectional decomposition when $u > 0$, and unidirectional decomposition when $u \leqslant 0$.

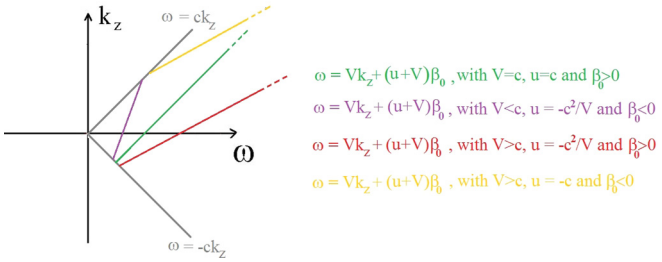

FIG. 1. The semi-straight lines and the line segment given by $\beta = \beta_0 \rightarrow \omega = Vk_z + (u+V)\beta_0$ which define the different types of ideal nondiffracting pulses. The values chosen for u are those that make easier the exact integration of Eq. (3).

In the new coordinates, the integral solution (1), after an integration on k_ρ, can be written as

$$\psi(\rho,\zeta,\eta) = \int_{\alpha_{\min}}^{\alpha_{\max}} d\alpha \int_{\beta_{\min}}^{\beta_{\max}} d\beta\, S(\alpha,\beta) J_0(\rho s(\alpha,\beta)) e^{-i\beta\eta} e^{i\alpha\zeta}, \tag{3}$$

where

$$s(\alpha,\beta) = \sqrt{\left(\frac{V^2}{c^2}-1\right)\alpha^2 + \left(\frac{u^2}{c^2}-1\right)\beta^2 + 2\left(\frac{uV}{c^2}+1\right)\alpha\beta} \tag{4}$$

and $S(\alpha,\beta)$ is the spectral function, with the new spectral parameters α and β given by

$$\alpha = \frac{1}{u+V}(\omega + uk_z), \qquad \beta = \frac{1}{u+V}(\omega - Vk_z). \tag{5}$$

The limits of the integrals in Eq. (3) depend on the values of V and u and define the allowed values of α and β in order to avoid evanescent waves. In the plane (ω,k_z), these values correspond to the region between the straight lines $\omega = ck_z$ and $\omega = -ck_z$. To make the derivation of exact analytical solutions easier, we can choose a subdomain of the allowed values, considering, for instance, the first and fourth quadrants of the plane (ω,k_z).

Now, with the integral representation (1) it is quite simple to consider spectra that fix a relation of the type $\omega = Vk_z + b$ which, as we have said, yield ideal nondiffracting pulses. For this, with the new spectral parameters, we just need a new spectral function of the type

$$S(\alpha,\beta) = \delta(\beta - \beta_0) A(\alpha,\beta), \tag{6}$$

with β_0 a constant. Due to the Dirac delta function $\delta(\beta - \beta_0)$ in the spectrum, the integral expression (3) becomes a superposition of zero-order Bessel beams with ω and k_z lying on the straight line[1] $\omega = Vk_z + (u+V)\beta_0$. The pulse peak velocity will be given by V and can be subluminal ($V < c$), luminal ($V = c$), or superluminal ($V > c$). The value of u in the decomposition (2) can be chosen to facilitate the analytical and exact integration of (3).

On the first and fourth quadrants of the plane (ω,k_z), Fig. 1 shows the semi-straight lines and the line segment given by $\beta = \beta_0$ which define the different types of ideal nondiffracting pulses.

By using Eq. (6), with $\beta_{\min} < \beta_0 < \beta_{\max}$, in (3) we get

$$\psi(\rho,\zeta,\eta) = e^{-i\beta_0\eta} \int_{\alpha_{\min}}^{\alpha_{\max}} d\alpha A(\alpha,\beta_0) J_0(\rho s(\alpha,\beta_0)) e^{i\alpha\zeta}. \tag{7}$$

In general, the spectra $A(\alpha,\beta_0)$ used in the localized wave theory yield pulses centered on $\zeta = 0 \rightarrow z = Vt$. Below we list several important nondiffracting pulses obtained from Eq. (7).

(1) Subluminal MacKinnon-type pulse:

$$\psi(\rho,\zeta,\eta) = \mathcal{N} e^{-i\beta_0\eta} \operatorname{sinc}\left(\frac{c}{V}|\beta_0|\sqrt{\gamma^{-2}\rho^2 - (a_1 + i\zeta)^2}\right), \tag{8}$$

where $a_1 > 0$, $\gamma = (1 - V^2/c^2)^{-1/2}$, and $\mathcal{N} = -2a_1 c\beta_0 \exp(a_1 c\beta_0/V)/\{V[1 - \exp(2a_1 c\beta_0/V)]\}$.

This pulse [11,17–20] is obtained from Eq. (7) considering $V < c, u = -c^2/V, \beta_0 < 0, \alpha_{\min} = c\beta_0/V, \alpha_{\max} = -c\beta_0/V$, and $A(\alpha,\beta_0) = -V\mathcal{N}/(2c\beta_0)\exp(a_1\alpha)$.

It is possible to show [20] that in order to minimize the contribution of the backward components to this solution it is necessary that $a_1 \gg V/[|\beta_0(c+V)|]$. It is also possible to show that, with this condition on a_1, the central angular frequency of this pulse is $\omega_c \approx c^2(V/c+1)|\beta_0|/V$, with a frequency bandwidth $\Delta\omega \approx V/a_1$.

The modulus square of the Mackinnon pulse is undistorted during the propagation, with a spot size of radius $\Delta\rho_0 = \gamma\sqrt{(\pi V/|\beta_0|c)^2 + a_1^2}$.

(2) The luminal focus wave mode (FWM):

$$\psi(\rho,\zeta,\eta) = a_1 \frac{e^{-i\beta_0\eta}}{a_1 - i\zeta} \exp\left(-\frac{\beta_0\rho^2}{a_1 - i\zeta}\right). \tag{9}$$

This pulse [6] is obtained from Eq. (7) considering $V = c, u = c, \beta_0 > 0, \alpha_{\min} = 0, \alpha_{\max} = \infty$, and $A(\alpha,\beta_0) = a_1\exp(-a_1\alpha)$, with $a_1 > 0$ a constant.

It is possible to show [21,22] that the central frequency of this pulse is $\omega_c = c\beta_0 + c/2a_1$, with a bandwidth $\Delta\omega \approx c/a_1$. It is also possible to show [6,21,22] that in order to minimize the contribution of the backward (wave) components of this solution (i.e., to make it causal) it is necessary that $a_1 \ll 1/\beta_0$, which implies that $\Delta\omega \approx 2\omega_c$. Such wideband frequency spectrum is a necessary condition to ensure the causality of the FWM pulse. This may give the wrong idea that luminal nondiffracting pulses must be ultrashort. Actually, although it is the case for the FWM solution, the existence of completely causal luminal nondiffracting pulses with arbitrary frequency bandwidths is quite possible and the only issue is that we do not know exact analytical solutions for these cases, which of course can be obtained through numerical simulations.

The modulus square of the FWM pulse is undistorted during the propagation, with a spot size of radius $\Delta\rho_0 = \sqrt{a_1/(2\beta_0)}$.

[1]This can be understood by noting that the Dirac delta function forces the condition $\beta = \beta_0 \rightarrow \omega = Vk_z + (u+V)\beta_0$.

(3) The superluminal focus wave mode (SFWM):

$$\psi(\rho,\zeta,\eta) = \mathcal{N}\frac{e^{-i\beta_0\eta}}{\sqrt{\gamma'^{-2}\rho^2+(a_1-i\zeta)^2}} \times \exp\left(-\frac{c}{V}\beta_0\sqrt{\gamma'^{-2}\rho^2+(a_1-i\zeta)^2}\right), \quad (10)$$

where $a_1 > 0$, $\gamma' = (V^2/c^2-1)^{-1/2}$ and $\mathcal{N} = a_1\exp(a_1 c\beta_0/V)$. This pulse [11–13] is obtained from Eq. (7) considering $V > c, u = -c^2/V, \beta_0 > 0, \alpha_{\min} = c|\beta_0|/V, \alpha_{\max} = \infty$, and $A(\alpha,\beta_0) = \mathcal{N}\exp(-a_1\alpha)$.

It is possible to show [6,11,12] that to minimize the contribution of the backward components to this solution it is necessary that $a_1 \ll V/[(V-c)\beta_0]$. It is also possible to show that the central frequency of this pulse is $\omega_c = (1-c/V)c\beta_0 + V/(2a_1)$, with an angular frequency bandwidth $\Delta\omega = V/a_1$ which, due to the condition on a_1, can be approximated by $\Delta\omega \approx 2\omega_c$. The ultra wideband frequency spectrum also occurs here but, as in the luminal case, it is not a fundamental characteristic of superluminal nondiffracting pulses as we will see in the next case.

The modulus square of the SFWM pulse is undistorted during the propagation, with a spot size of radius $\Delta\rho_0 = \gamma'\sqrt{[a_1+V/(2c\beta_0)]^2-a_1^2}$.

(4) The superluminal focus wave mode totally free of backward components:

$$\psi(\rho,\zeta,\eta) = a_1 X e^{-i\beta_0\eta}\exp\left[-\frac{\beta_0}{\frac{V}{c}+1}\left(a_1-i\zeta-X^{-1}\right)\right], \quad (11)$$

where $X = [\gamma'^{-2}\rho^2+(a_1-i\zeta)^2]^{-1/2}$ is the classical X-wave solution, $a_1 > 0$, and $\gamma' = (V^2/c^2-1)^{-1/2}$. This pulse [13] is obtained from Eq. (7) considering $V > c$, $u = -c$, $\beta_0 < 0$, $\alpha_{\min} = 0$, $\alpha_{\max} = \infty$, and $A(\alpha,\beta_0) = a_1\exp(-a_1\alpha)$. It possesses a central frequency $\omega_c = c|\beta_0| + V/(2a_1)$, with an angular frequency bandwidth $\Delta\omega = V/a_1$. It is important to note that this pulse solution is totally free of backward components, which is a great advantage. Due to this, it can possess any time width, not necessarily characterized by wide-frequency bandwidths as is usually the case with other nondiffracting pulses of known analytical solutions.

The modulus square of this pulse is undistorted during the propagation, with a spot size of radius $\Delta\rho_0 \approx \gamma' a_1\sqrt{(V/c+1)^2/(4\beta_0^2a_1^2)+(V/c+1)/(a_1|\beta_0|)}$ in the case $a_1|\beta_0| > (V/c+1)/(2\sqrt{2}-2)$, otherwise we have $\Delta\rho_0 \approx \gamma' a_1$.

The intensities of all the pulses described above are undistorted for all time. Actually, this is the basic characteristic of all known ideal nondiffracting pulses (and beams) which, as we have already said, possess infinite energy. The latter drawback can be addressed by truncating [23–25] the ideal solutions[2] (finite aperture generation) or by concentrating the spectrum $A'(k_\rho,k_z,\omega)$ entering Eq. (1) in a region surrounding the straight line $\omega = Vk_z + b$ instead of collapsing it exactly over that line [6,11–13]. In both cases, the resulting waves attain finite energy and are resistant to the diffraction effects for long (but not infinite) distances.

In the next section we are going to take a step forward in the theory of the localized waves by introducing a method that will enable us to model the space-time focusing of ideal nondiffracting pulses.

III. THE METHOD FOR MODELING THE SPACE-TIME FOCUSING OF IDEAL NONDIFFRACTING PULSES

In general, the peak of an ideal nondiffracting pulse with azimuthal symmetry, $\psi(\rho,\zeta,\eta)$, occurs at

$$\rho = 0 \text{ and } \zeta = 0 \text{ (i.e., } z = Vt) \rightarrow \eta = \left(1+\frac{u}{V}\right)z \equiv \left(1+\frac{u}{V}\right)z_p, \quad (12)$$

where we have used Eq. (2) and called $z = z_p$, z_p being the peak's z position. In this case, the pulse's peak based on Eq. (7) is described by

$$\psi[\rho=0,\zeta=0,\eta=(1+u/V)z_p] = \exp\left[-i\left(1+\frac{u}{V}\right)\beta_0 z_p\right]\int_{\alpha_{\min}}^{\alpha_{\max}} d\alpha A(\alpha,\beta_0). \quad (13)$$

Next, a new pulse solution, Ψ, will be constructed in such a manner that both the position of its peak, as well as the intensity of the peak, can be chosen within a longitudinal spatial range $0 \leqslant z \leqslant L$. The new pulse is defined as a superposition of localized wave pulses like those in Eq. (7), with the same spectral function $A(\alpha,\beta_0)$ but with values of β different from β_0, in such a way that we can write for the new solution:

$$\Psi[\rho=0,\zeta=0,\eta=(1+u/V)z_p] \equiv \sum_{n=-N}^{N} B_n U_n \exp\left[-i\left(1+\frac{u}{V}\right)\beta_n z_p\right], \quad (14)$$

where $U_n = \int_{\alpha_{\min}}^{\alpha_{\max}} d\alpha\, A(\alpha,\beta_n)$, with the coefficients B_n and the values of β_n yet unknown.

If the choices

$$\beta_n = \frac{1}{1+u/V}\left(Q+\frac{2\pi}{L}n\right) \quad (15)$$

and

$$B_n = \frac{1}{LU_n}\int_0^L F(z_p)e^{i(2\pi n/L)z_p}dz_p \quad (16)$$

are made, with Q and $F(z_p)$ a constant and an arbitrary function, respectively, the intensity of the expression in Eq. (14) within $0 \leqslant z_p \leqslant L$ will result in

$$|\Psi[\rho=0,\zeta=0,\eta=(1+u/V)z_p]|^2 \approx |F(z_p)|^2 \quad (17)$$

and so we can choose, through the function $F(z_p)$, the locations and how intense the pulse's peak will appear.

The three-dimensional (3D) *exact solution* is given by

$$\Psi(\rho,\zeta,\eta) = \sum_{n=-N}^{N} B_n\psi_n(\rho,\zeta,\eta), \quad (18)$$

[2]In this case the resulting field is given by diffraction integrals, which rarely can be solved analytically.

where

$$\psi_n(\rho,\zeta,\eta) = e^{-i\beta_n\eta}\int_{\alpha_{\min}}^{\alpha_{\max}} A(\alpha,\beta_n)J_0(\rho s(\alpha,\beta_n))e^{i\alpha\zeta}. \quad (19)$$

This approach is different from the ordinary space and time focusing methods, such as those developed in [14–16], where there is just one point of focalization. It is a much more powerful method because, we repeat, it allows us to choose multiple locations (spatial ranges) of space and time focalization, where the pulse intensities also can be chosen *a priori*. This technique can be seen as a pulsed version of the frozen wave method [26–31] (originally developed for beams) and it can be implemented for subluminal, luminal, and superluminal pulsed solutions. It is important to note that within all focal lines, the resulting pulses will be nondiffracting. It is also important to stress that, with the present method, the very complex task of modeling the space-time behavior of nondiffracting pulses is reduced to a very simple problem of finding the Fourier coefficients of $F(z_p)$.

In general, the nondiffracting pulses ψ_n given in Eq. (19), and used in the new solution (18), have all their β_n with the same sign, positive or negative. Once we have chosen the value of β_0 [which in turn defines the value of Q via Eq. (15)] and L, this fact will imply a maximum value allowed for N, which restricts the number $2N+1$ of terms in the fundamental superposition (18). The maximum value of N can be obtained from Eq. (15), with the requirement that all β_n have to possess the same sign (positive or negative) of the chosen β_0.

It is not difficult to show that in any case the maximum value of N in (18) has to obey

$$N \leqslant \frac{|1+u/V|}{2\pi}L|\beta_0|. \quad (20)$$

With the method in hand, a natural question emerges: Which criteria should be used in choosing the value of the parameter β_0, which determines Q through Eq. (15), L, and any other appearing within the spectral function $A(\alpha,\beta_n)$ in Eq. (19), which defines ψ_n?

First we have to say that any new solution $\Psi(\rho,\zeta,\eta)$, given by Eq. (18), will have several important characteristics associated to it, such as a central frequency, frequency bandwidth, and the transverse spot size, which will be approximately similar to those presented by the central pulse, ψ_0, of the superposition (18). These characteristics of ψ_0 are described by equations involving the parameter β_0 and those occurring in $A(\alpha,\beta_0)$, which, therefore, can be determined once the desired characteristics mentioned above are chosen.[3]

The value of L cannot be evaluated in this way, but a good criterion is to choose it taking as reference the diffraction length, Z_{Gauss} of a Gaussian pulse possessing the same spot size of the desired new pulse. Good choices for L would be those limited to values not much greater than 100 or 1000 times the value of Z_{Gauss}, otherwise we risk dealing with unrealistic situations in experimental apparatus sizes to generate the finite-energy version of the pulse.

Having presented our method, we are going to illustrate it with a few examples, which will confirm its efficiency and simplicity. It is important to notice that in the following examples some of the desired pulse peak evolution patterns involve step functions, which are discontinuous. However, the resulting pulses will not present any discontinuities because they are given by a discrete and finite superposition of continuous pulsed solutions [see Eq. (18)]. Actually, what we are going to get are resulting pulses that approach the desired patterns, maintaining, however, the necessary properties of continuity and differentiability.

First example. Here, we shall model the space-time focusing of a subluminal nondiffracting pulse. To do this, we are going to use the fundamental solution (18), with the ψ_n given by the subluminal MacKinnon solution in Eq. (8), with β_0 replaced with β_n.

In this case, we can set the parameters β_0 [which defines Q through Eq. (15)] and a_1 according to the central frequency and frequency bandwidth of the resulting pulse, remembering that these characteristics are approximately similar to those of the central pulse ψ_0 of the superposition (18). In this case, ψ_0 is given by the Mackinnon-type solution, Eq. (8), whose characteristics cited above were presented in the previous section.

Considering a peak velocity $V = 0.999c$, with $u = -c^2/V$, a central angular frequency $\omega_c = 2.98\times10^{15}$ rad/s and a frequency bandwidth $\Delta\omega \approx 10^{-2}\omega_c$, we can get $\beta_0 = -4.96\times10^6\ \text{m}^{-1}$ and $a_1 = 1.01\times10^{-5}$ m. With this, the intensity spot radius for the resulting pulse can be estimated as being $\Delta\rho_0 \approx 0.226$ mm. Concerning the value of L, which defines the range $0 \leqslant z_p \leqslant L$ within which the space-time modeling will be made, we note that an ordinary (Gaussian) pulse with the same spot size considered here would possess a diffraction length $Z_{\text{diff}} = 0.14$ m so, according to our previous considerations, the value of L should not be many orders of magnitude greater than this value for avoiding unrealistic situations. Let us choose $L = 30Z_{\text{diff}} \approx 4.2$ m.

For the function $F(z_p)$, whose modulus square will shape the positions and intensity of the resulting pulse's peak in the range $0 \leqslant z_p \leqslant L$, let us choose a ladder intensity pattern on the space interval $L/3 \leqslant z_p \leqslant 2L/3$, and zero outside it. More specifically, we wish that within $0 \leqslant z \leqslant L$ the pulse's peak intensity obeys $|\Psi[\rho=0,\zeta=0,\eta=(1+u/V)z_p]|^2 \approx |F(z_p)|^2$, with

$$F(z_p) = \begin{cases} 1 & \text{for } l_1 < z_p < l_2 \\ \sqrt{2} & \text{for } l_2 < z_p < l_3 \\ \sqrt{3} & \text{for } l_3 < z_p < l_4 \\ 0 & \text{otherwise.} \end{cases} \quad (21)$$

Here, $l_1 = L/3$, $l_2 = L/3+\Delta l$, $l_3 = L/3+2\Delta l$, and $l_4 = L/3+3\Delta l$, with $\Delta l = L/9$.

The resulting pulse is given by Eq. (18) with the coefficients B_n given by Eq. (16) and ψ_n given by Eq. (8) through the replacement $\beta_0 \to \beta_n$, with β_n given by Eq. (15). Here, the maximum allowed value for N is 6,616, but we will use $N = 60$.

[3] In general, just the central frequency and the frequency bandwidth or just the central frequency and the spot size are necessary to determine the value of β_0 and the values of other possible parameters occurring in $A(\alpha,\beta_0)$.

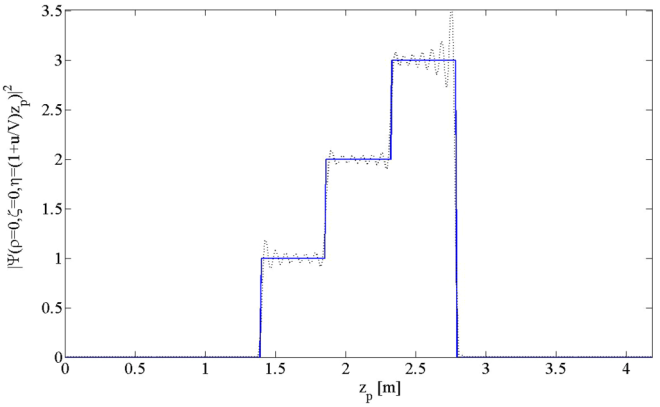

FIG. 2. The peak intensity evolution, $|\Psi[\rho = 0,\zeta = 0,\eta = (1 + u/V)z_p]|^2$, of the resulting subluminal pulse is shown by a dotted line, while the desired peak intensity evolution for it, $|F(z_p)|^2$, is shown by a continuous line. Good agreement between them is observed.

Figure 2 shows, within the range $0 \leqslant z_p \leqslant L$, the evolution of the actual pulse's peak intensity, $|\Psi[\rho = 0,\zeta = 0,\eta = (1 + u/V)z_p]|^2$, using a dotted line and the desired spatial evolution for it, $|F(z_p)|^2$, using a continuous line. We can see good agreement between them.

Even more interesting is Fig. 3, which shows the 3D pulse intensity, $|\Psi(\rho,\zeta,\eta)|^2$, at nine different instants of time. More specifically, the first, second, and third lines of the subfigures show the pulse evolution within the ranges $0 < z < L/3$, $L/3 < z < 2L/3$, and $2L/3 < z < L$, respectively. It is very clear that the resulting nondiffracting pulse possesses the desired space-time focusing characteristics.

Second example. Next, we are going to model the space-time focusing of a luminal nondiffracting pulse. For this, we will use our fundamental solution (18) with the ψ_n given by the luminal FWM solution, Eq. (9), with β_0 replaced by β_n.

In this case, the parameters β_0 and a_1 are chosen according to the desired central frequency and transverse spot size for the resulting pulse, these characteristics being approximately similar to those of the central pulse ψ_0 of the superposition (18). In this case, ψ_0 is given by the FWM solution, Eq. (9), of which the characteristics cited above were presented in the previous section.

Considering for the resulting pulse a peak velocity $V = c$, with $u = c$, a central angular frequency $\omega_c = 2.98 \times 10^{15}$ rad/s and an intensity spot radius $\Delta\rho_0 = 10\ \mu$m, we obtain $\beta_0 = 2.518 \times 10^2\ \text{m}^{-1}$ and $a_1 = 5.036 \times 10^{-8}$ m. In this case the frequency bandwidth is $\Delta\omega \approx 2\omega_c$. Furthermore, we choose $L = 0.516$ m, which is 300 times greater than the diffraction length of a Gaussian pulse with the same spot size considered here.

Within the region $0 \leqslant z_p \leqslant L$ the pulse's peak intensity evolution obeys $|\Psi[\rho = 0,\zeta = 0,\eta = (1 + u/V)z_p]|^2 \approx |F(z_p)|^2$, with the choice

$$F(z_p) = \begin{cases} 1/\sqrt{2} & \text{for } 0 < z_p < L/3 \\ 0 & \text{for } L/3 < z_p < 2L/3 \\ 1 & \text{for } 2L/3 < z_p < L. \end{cases} \tag{22}$$

The resulting pulse is given by Eq. (18) with the coefficients B_n given by Eq. (16) and ψ_n given by Eq. (9) through the replacement $\beta_0 \to \beta_n$, with β_n given by Eq. (15). Here, we use $N = 30$.

Figure 4 shows, within the range $0 \leqslant z_p \leqslant L$, a good agreement between the actual pulse's peak intensity evolution, $|\Psi[\rho = 0,\zeta = 0,\eta = (1 + u/V)z_p]|^2$, (dotted line) and the desired spatial evolution, $|F(z_p)|^2$, for it (continuous line).

Figure 5 shows the 3D evolution of the pulse intensity, $|\Psi(\rho,\zeta,\eta)|^2$, at nine different instants of time. The first, second, and third lines of the subfigures show the pulse evolution within the ranges $0 < z < L/3$, $L/3 < z < 2L/3$, and $2L/3 < z < L$, respectively. It is clear that the resulting nondiffracting pulse possesses the desired space-time focusing characteristics.

Third example. Finally, we shall model the space-time focusing of a superluminal nondiffracting pulse. Again, we use our fundamental solution (18), but now with the ψ_n given

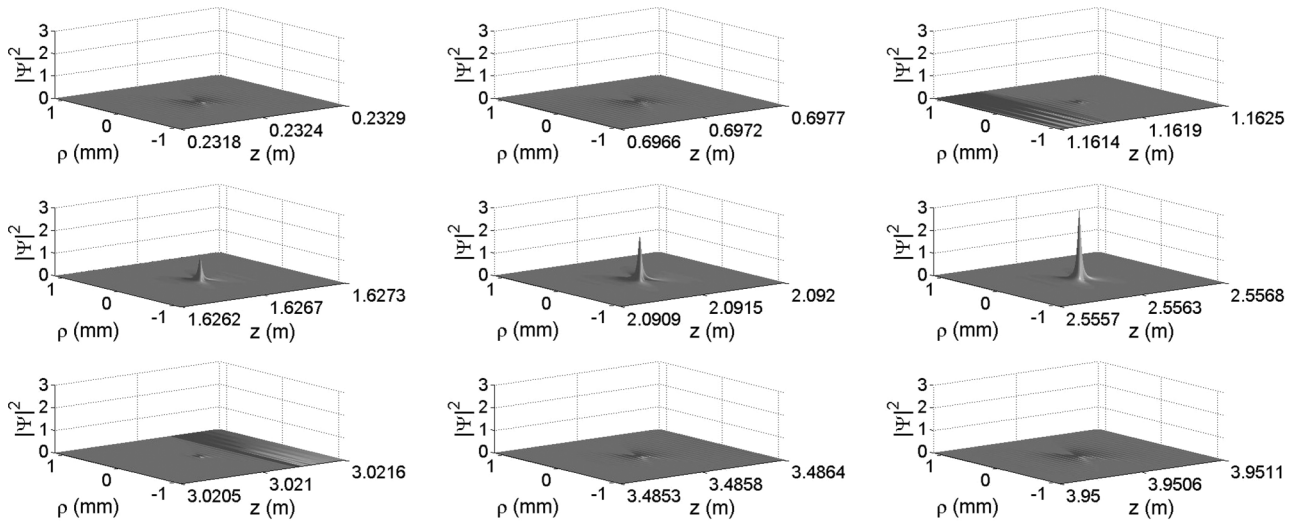

FIG. 3. The 3D pulse intensity, $|\Psi(\rho,\zeta,\eta)|^2$, for the resulting subluminal pulse at nine different instants of time. The first, second, and third lines of the subfigures show the pulse evolution within the ranges $0 < z < L/3$, $L/3 < z < 2L/3$, and $2L/3 < z < L$, respectively. We can see that the resulting nondiffracting pulse possesses the desired space-time focusing characteristics.

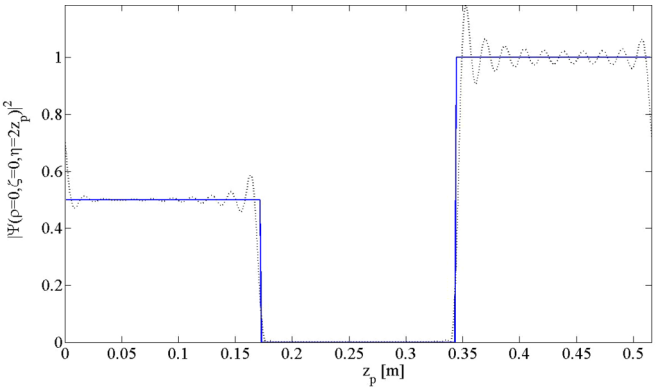

FIG. 4. The peak intensity evolution, $|\Psi[\rho = 0, \zeta = 0, \eta = (1 + u/V)z_p]|^2$, of the resulting luminal pulse is shown by a dotted line, while the desired peak intensity evolution for it, $|F(z_p)|^2$, is shown by a continuous line. Good agreement between them is seen.

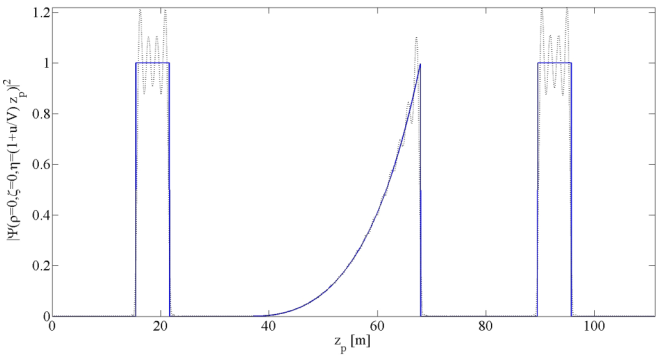

FIG. 6. The peak intensity evolution, $|\Psi[\rho = 0, \zeta = 0, \eta = (1 + u/V)z_p]|^2$, of the resulting superluminal pulse is shown by a dotted line, while the desired peak intensity profile for it, $|F(z_p)|^2$, is shown by a continuous line. Good agreement between them is observed.

by the superluminal solution in Eq. (11) with β_0 replaced with β_n.

Considering a peak velocity $V = 1.0001c$, with $u = -c$, a central angular frequency $\omega_c = 2.98 \times 10^{15}$ rad/s, a frequency bandwidth $\Delta\omega = \omega_c/10^3$, and following the same procedure as in the previous examples, but now considering ψ_0 as given by Eq. (11), we can get $\beta_0 = -9.9242 \times 10^6$ m^{-1} and $a_1 = 1.0072 \times 10^{-4}$ m. In this case, the intensity spot radius for the resulting picosecond pulse can be estimated as being $\Delta\rho_0 \approx 0.32$ mm. We also choose $L = 111.2$ m, which is approximately 400 times greater than the diffraction length of a Gaussian pulse with the same spot size considered here.

For the space-time focusing modeling within $0 \leqslant z \leqslant L$, we wish the superluminal pulse's peak intensity $|\Psi[\rho = 0, \zeta = 0, \eta = (1 + u/V)z_p]|^2 \approx |F(z_p)|^2$ to behave as

$$F(z_p) = \begin{cases} 1 & \text{for } l_1 < z_p < l_2 \\ \frac{\exp[(z-l_3)/(l_4-l_3)]-1}{e-1} & \text{for } l_3 < z_p < l_4 \\ 1 & \text{for } l_5 < z_p < l_6, \end{cases} \quad (23)$$

where $l_1 = 1.25\Delta l$, $l_2 = 1.75\Delta l$, $l_3 = 3\Delta l$, $l_4 = 5.5\Delta l$, $l_5 = 7.25\Delta l$, and $l_6 = 7.75\Delta l$, with $\Delta l = L/9$. This desired pattern for the evolution of the pulse's peak intensity is shown in Fig. 6 by a continuous line.

The resulting pulse is given by Eq. (18) with the coefficients B_n given by Eq. (16) and ψ_n given by Eq. (11) through the replacement $\beta_0 \to \beta_n$, with β_n given by Eq. (15). Here, we use $N = 70$.

Figure 6 shows, using a dotted line, the actual pulse's peak intensity profile along the axis, $|\Psi[\rho = 0, \zeta = 0, \eta = (1 + u/V)z_p]|^2$, which presents good agreement with the desired pattern (continuous line).

Figure 7 shows the 3D evolution of the pulse intensity, $|\Psi(\rho, \zeta, \eta)|^2$, at nine different instants of time. The first, second, and third lines of the subfigures show the pulse evolution within the ranges $0 < z < L/3$, $L/3 < z < 2L/3$, and $2L/3 < z < L$, respectively. Again, it is clear that the resulting nondiffracting pulse possesses the desired space-time focusing characteristics.

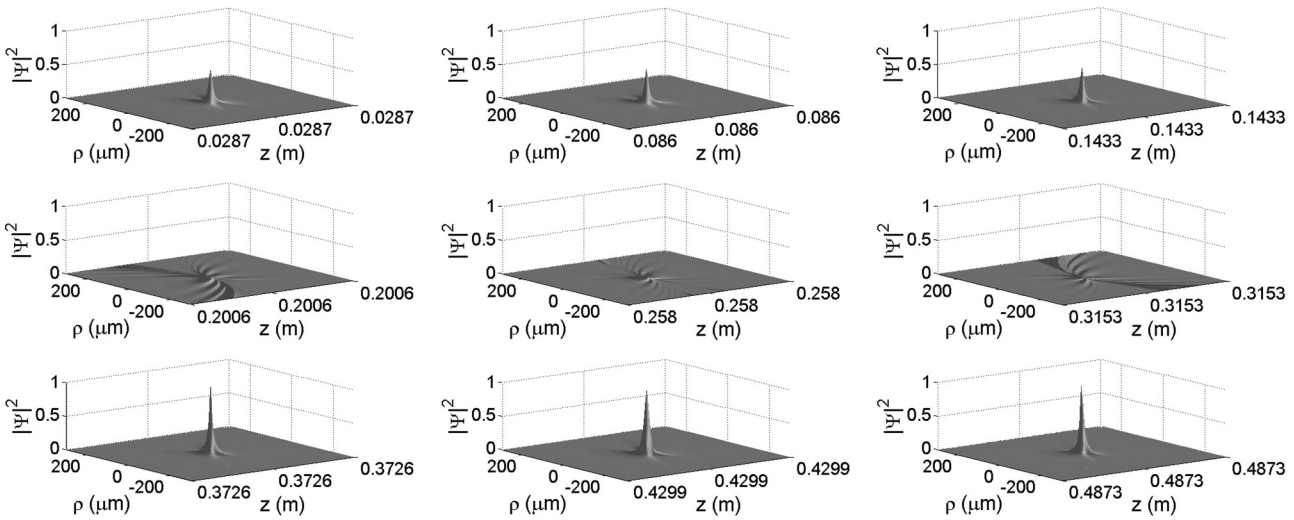

FIG. 5. The 3D pulse intensity, $|\Psi(\rho, \zeta, \eta)|^2$, for the resulting luminal pulse at nine different instants of time. The first, second, and third lines of the subfigures show the pulse evolution within the ranges $0 < z < L/3$, $L/3 < z < 2L/3$, and $2L/3 < z < L$, respectively. We can see that the resulting nondiffracting pulse possesses the desired space-time focusing characteristics.

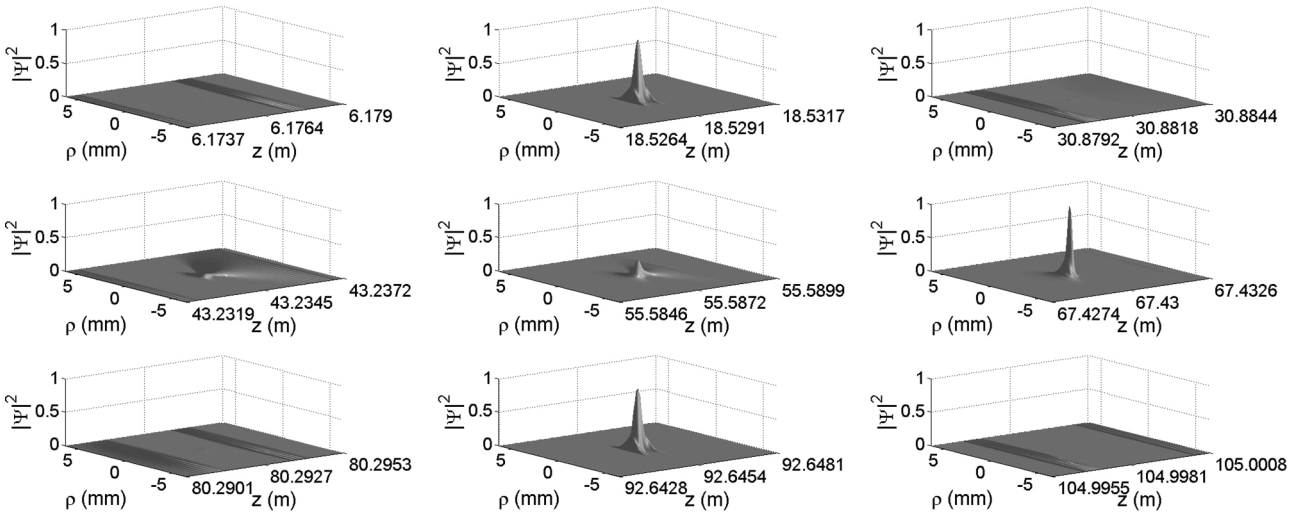

FIG. 7. The 3D pulse intensity, $|\Psi(\rho,\zeta,\eta)|^2$, for the resulting superluminal pulse at nine different instants of time. The first, second, and third lines of the subfigures show the pulse evolution within the ranges $0 < z < L/3$, $L/3 < z < 2L/3$, and $2L/3 < z < L$, respectively. We can see that the resulting nondiffracting pulse possesses the desired space-time focusing characteristics.

IV. THE FINITE-ENERGY VERSION OF THE METHOD

The method presented in the previous sections for modeling the space and time evolution of localized wave pulses is based on suitable and discrete superposition of ideal nondiffracting pulses. As a consequence, the resulting solutions also present infinite energy content.

This physical deficiency can be addressed in a very simple and effective way by replacing the ideal nondiffracting pulses, ψ_n, with their finite-energy versions in the fundamental superposition (18), followed by specific changes in the respective series coefficients. The result is a finite-energy version of our method, as we are going to show below.

Given an ideal nondiffracting pulse, whose spectrum $A'(k_\rho,k_z,\omega)$ assumes values different from zero only over a straight line of the type $\omega = Vk_z + b$, it is possible to obtain a finite-energy version of it by concentrating the original spectrum in the surrounding of that straight line, instead of collapsing it exactly over that line. In this case, the resulting pulse possesses finite energy and is endowed with a finite field depth, i.e., it maintains its spatial form for long, but not infinite, distances. The more concentrated on the straight line is the spectrum, the greater the depth of field of the resulting pulse (demanding more energy, naturally).

That approach was used in a series of papers [6,9–13], providing many exact analytical solutions of finite-energy localized wave pulses.

Now, a finite version of our method can be constructed following the two steps below:

(1) In the fundamental superposition (18), we replace the ideal nondiffracting pulses, ψ_n, with their finite-energy versions.

(2) The series coefficients B_n are now defined as

$$B_n = \frac{1}{LU_n}\int_0^L \frac{F(z_p)}{G(z_p)} e^{i(2\pi n/L)z_p} dz_p, \tag{24}$$

where $G^2(z_p)$ is the (average) peak intensity decreasing factor of the finite-energy pulses, ψ_n, along z. In effect, what we have used is a compensation scheme: with the new coefficients B_n in (18), the resulting pulse will have the positions and intensities of its peak, in the range $0 \leqslant z_p \leqslant L$, given approximately by $|F(z_p)/G(z_p)|^2|G(z_p)|^2 = |F(z_p)|^2$, which is the desired result.

To exemplify the efficiency of the extended method, we apply it to obtain the finite-energy version of example 2 of the third section.

A finite-energy version of the FWM pulse, Eq. (9), is the so-called modified power spectrum (MPS) pulse [6], given by

$$\psi(\rho,\zeta,\eta) = \frac{a_1 a_2\, e^{-i\beta_0\eta}}{(a_1 - i\zeta)\left(a_2 + i\eta + \frac{\rho^2}{a_1 - i\zeta}\right)} \exp\left(-\frac{\beta_0\rho^2}{a_1 - i\zeta}\right). \tag{25}$$

The MPS pulse is obtained from (3) with $V = c, u = c, \beta_{\min} = 0, \beta_{\max} = \infty, \alpha_{\min} = 0, \alpha_{\max} = \infty$, and

$$S(\alpha,\beta) = a_1 a_2 \exp(a_2\beta_0)\exp(-a_1\alpha)\exp(-a_2\beta)H(\beta - \beta_0), \tag{26}$$

with a_1 and a_2 positive constants, $\beta_0 > 0$, and $H(\cdot)$ the Heaviside function. Such a spectrum is exponentially concentrated on the line $\omega = ck_z + 2c\beta_0$.

It is easy to see that the peak intensity of the MPS pulse occurs at $\rho = 0$ and $\zeta = 0 \to \eta = 2z \equiv 2z_p$, and it is given by

$$|\psi(\rho = 0,\zeta = 0,\eta = 2z_p)|^2 = \frac{a_2^2}{a_2^2 + 4z_p^2} \equiv G^2(z_p), \tag{27}$$

which implies a field depth approximately equal to $a_2\sqrt{e-1}/2$.

Now, to obtain the finite-energy version of the space-time focusing modeling given in the second example of the previous section, we consider the same parameter values given there and the same $F(z_p)$, replacing, in the fundamental superposition (18), the ψ_n given by the FWM pulse with the MPS pulse

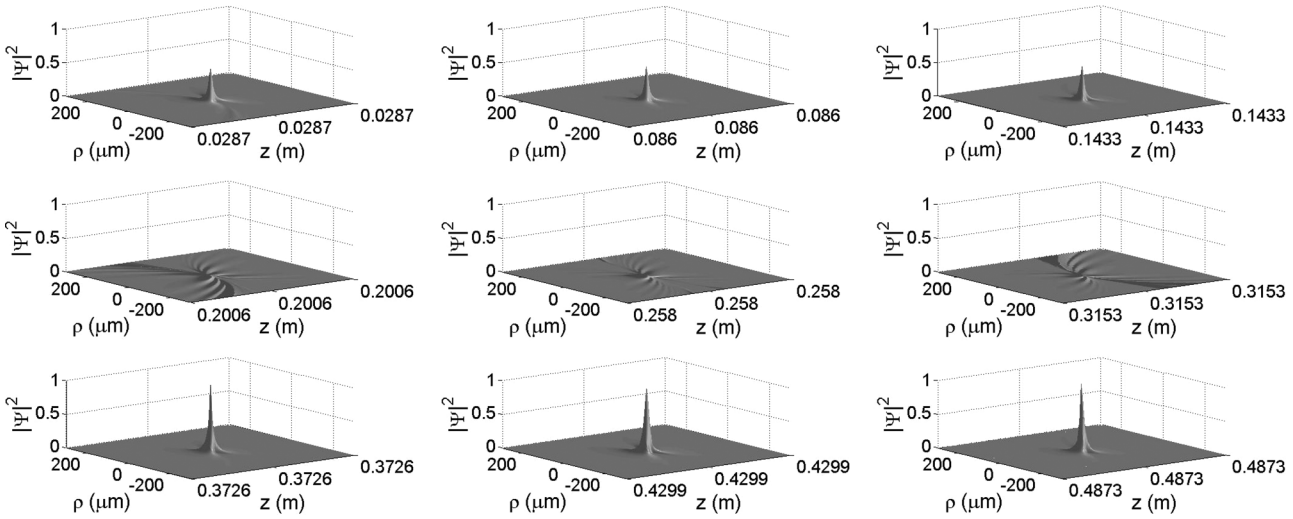

FIG. 8. The 3D pulse intensity, $|\Psi(\rho,\zeta,\eta)|^2$, for the resulting finite-energy luminal pulse at nine different instants of time. The first, second, and third lines of the subfigures show the pulse evolution within the ranges $0 < z < L/3$, $L/3 < z < 2L/3$, and $2L/3 < z < L$, respectively. The resulting diffraction resistant pulse with finite energy possesses the desired space-time focusing characteristics.

given by Eq. (25), with β_0 replaced by β_n, which are given by Eq. (15). Furthermore, the coefficients B_n now are given by Eq. (24), with

$$G(z_p) = \sqrt{\frac{a_2^2}{a_2^2 + 4z_p^2}}. \tag{28}$$

In this case, we choose $a_2 = 0.7872$ m.

Figure 8 shows the 3D evolution of the finite-energy pulse intensity, $|\Psi(\rho,\zeta,\eta)|^2$, at nine different instants of time. The first, second, and third lines of the subfigures show the pulse evolution within the ranges $0 < z < L/3$, $L/3 < z < 2L/3$, and $2L/3 < z < L$, respectively. It is clear that the resulting finite-energy diffraction resistant pulse possesses the desired space-time focusing characteristics.

We note from Figs. 5 and 8 that the ideal (infinite energy) luminal pulse and its finite-energy version possess no differences within the main range $0 \leqslant z \leqslant L$, where the space-time modeling was made. Now, for $z > L = 51.59$ cm, the differences between them come up, as we can see from Fig. 9, which shows the peak intensity evolution for both cases. While the peak of the ideal pulse presents a periodic spatial behavior, the peak of its finite-energy version shows an intensity decay with distance for $z > L = 51.59$ cm.

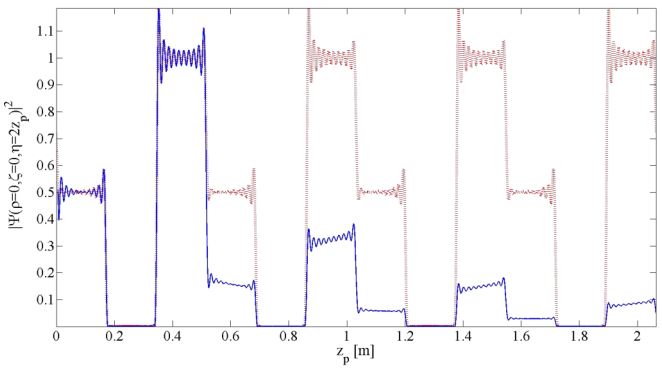

FIG. 9. The peak intensity evolution of the ideal luminal pulse (dotted line) of the second example and the peak evolution of its finite-energy version (continuous line). They are essentially the same within the main range, $0 \leqslant z \leqslant L = 51.59$ cm, where the space-time modeling was made, but for $z > L = 51.59$ cm, while the peak of the ideal pulse presents a periodic spatial behavior, the peak of its finite-energy version exhibits an intensity decay with distance.

V. CONCLUSIONS

In this paper, a method has been presented that enables the modeling of space and time focusing of nondiffracting pulses. Specifically, it has been shown how to construct localized pulse solutions in such a way that one can choose where and how intense their peaks will be within a longitudinal spatial range $0 \leqslant z \leqslant L$. This approach can be considered a step forward in the localized wave theory as it enables one to take advantage of the great potential of the nondiffracting wave pulses in a highly selective manner, by choosing *a priori* multiple locations (spatial ranges) of space and time focalization, with the pulse intensities also being chosen.

Space and time focusing modeling of ideal and of finite-energy localized nondiffracting pulses with subluminal, luminal, or superluminal peak velocities has been carried out by means of suitable superpositions of ideal and of finite-energy standard nondiffracting pulses. The resulting waves can have potential applications in many different fields, such as free-space optical communications, remote sensing, and medical apparatus, to name a few.

ACKNOWLEDGMENTS

The authors thank Mo Mojahedi and Ahmed Dorrah for valuable discussions and kind collaboration. This work was supported by Fundação de Amparo à Pesquisa do Estado de São Paulo (FAPESP) (under Grant No. 2015/26444-8) and by Conselho Nacional de Desenvolvimento Científico e Tecnológico (CNPq) (under Grant No. 312376/2013-8).

[1] C. J. R. Sheppard, Electromagnetic field in the focal region of wide-angular annular lens and mirror systems, IEE J. Microwaves, Opt. Acoust. **2**, 163 (1983).

[2] J. N. Brittingham, Focus wave modes in homogeneous Maxwell's equations: Transverse electric mode, J. Appl. Phys. **54**, 1179 (1983).

[3] A. P. Kiselev, Modulated Gaussian beams, Radiophys. Quantum Electron. (Engl. Transl.) **26**, 755 (1983).

[4] A. Sezginer, A general formulation of focus wave modes, J. Appl. Phys. **57**, 678 (1985).

[5] J. Durnin, J. J. Miceli, and J. H. Eberly, Diffraction-Free beams, Phys. Rev. Lett. **58**, 1499 (1987).

[6] I. M. Besieris, A. M. Shaarawi, and R. W. Ziolkowski, A bi-directional traveling plane wave representation of exact solutions of the scalar wave equation, J. Math. Phys. **30**, 1254 (1989).

[7] J.-y. Lu and J. F. Greenleaf, Experimental verification of nondiffracting X-waves, IEEE Trans. Ultrason. Ferroelectr. Freq. Control **39**, 441 (1992).

[8] R. Donnelly and R. W. Ziolkowski, Designing localized waves, Proc. R. Soc. London, Ser. A **440**, 541 (1993).

[9] *Localized Waves*, edited by H. E. Hernandez-Figueroa, Michel Zamboni-Rached, and E. Recami, 1st ed. (Wiley, Hoboken, NJ, 2008).

[10] *Non-Diffracting Waves*, edited by H. E. Hernandez Figueroa, E. Recami, and Michel Zamboni-Rached, 1st ed. (Wiley-VCH Verlag, Weinheim, 2014).

[11] I. M. Besieris, M. Abdel-Rahman, A. Shaarawi, and A. Chatzipetros, Two fundamental representations of localized pulse solutions of the scalar wave equation, Prog. Electromagn. Res. **19**, 1 (1998).

[12] M. Zamboni-Rached, E. Recami, and H. E. Hernández-Figueroa, New localized superluminal solutions to the wave equations with finite total energies and arbitrary frequencies, Eur. Phys. J. D **21**, 217 (2002).

[13] M. Zamboni-Rached, Unidirectional decomposition method for obtaining exact localized wave solutions totally free of backward components, Phys. Rev. A **79**, 013816 (2009).

[14] A. M. Shaarawi, I. M. Besieris and T. M. Said, Temporal focusing by use of composite X-waves, J. Opt. Soc. Am. A **20**, 1658 (2003).

[15] A. M. Shaarawi and I. M. Besieris, Focusing of ultra-wideband X waves, in *Ultra-Wideband, Short-Pulse Electromagnetics 6*, edited by E. L. Mokole, M. Kragalott, and K. R. Gerlach (Kluwer Academic Plenum Publishers, New York, 2003), pp. 193–202.

[16] Michel Zamboni-Rached, A. Shaarawi, and E. Recami, Focused X-shaped pulses, J. Opt. Soc. Am. A **21**, 1564 (2004).

[17] L. Mackinnon, A nondispersive de Broglie wave packet, Found. Phys. **8**, 157 (1978).

[18] J. Salo and M. M. Salomaa, Subsonic nondiffracting waves, Acoust. Res. Lett. Online **2**, 31 (2001).

[19] P. Saari and K. Reivelt, Generation and classification of localized waves by Lorentz transformations in Fourier space, Phys. Rev. E **69**, 036612 (2004).

[20] M. Zamboni-Rached and E. Recami, Subluminal wave bullets: Exact localized subluminal solutions to the wave equations, Phys. Rev. A **77**, 033824 (2008).

[21] M. Zamboni-Rached, Localized solutions: Structure and applications, M. Sc. thesis, Campinas State University, 1999.

[22] M. Zamboni-Rached, Localized waves in diffractive/dispersive media, Ph.D. thesis, Universidade Estadual de Campinas, DMO/FEEC, 2004.

[23] R. W. Ziolkowski, I. M. Besieris, and A. M. Shaarawi, Aperture realizations of exact solutions to homogeneous wave-equations, J. Opt. Soc. Am. A **10**, 75 (1993).

[24] Michel Zamboni-Rached, Analytical expressions for the longitudinal evolution of nondiffracting pulses truncated by finite apertures, J. Opt. Soc. Am. A **23**, 2166 (2006).

[25] Michel Zamboni-Rached, Erasmo Recami, and Massimo Balma, Simple and effective method for the analytic description of important optical beams when truncated by finite apertures, Appl. Opt. **51**, 3370 (2012)

[26] M. Zamboni-Rached, Stationary optical wave fields with arbitrary longitudinal shape by superposing equal frequency Bessel beams: Frozen waves, Opt. Express **12**, 4001 (2004).

[27] M. Zamboni-Rached, Diffraction-attenuation resistant beams in absorbing media, Opt. Express **14**, 1804 (2006).

[28] Tárcio A. Vieira, Marcos R. R. Gesualdi, and Michel Zamboni-Rached, Frozen waves: Experimental generation, Opt. Lett. **37**, 2034 (2012).

[29] Tárcio A. Vieira, Michel Zamboni-Rached, and Marcos R. R. Gesualdi, Modeling the spatial shape of nondiffracting beams: Experimental generation of frozen waves via holographic method, Opt. Commun. **315**, 374 (2014).

[30] J. L. Prego, M. Zamboni-Rached, E. Recami, and H. E. Hernandez-Figueroa, Producing acoustic frozen waves: Simulated experiments, IEEE Trans. Ultrason. Ferroelectr. Freq. Control **60**, 2414 (2013).

[31] J. L. Prego-Borgesa, Michel Zamboni-Rached, Erasmo Recami, and Eduardo Tavares Costa, Producing acoustic frozen waves: Simulated experiments with diffraction/attenuation resistant beams in lossy media, Ultrasonics **54**, 1620 (2014).